Applied Chemical Engineering (2026) Volume 9 Issue 3 ISSN: 2578-2010 (O)
doi: 10.59429/ace.v9i3.6132

ORIGINAL RESEARCH ARTICLE

Comparative study of the surface modification of chitosan using anionic surfactants for methylene blue adsorption.

Aya B. Mohsin*, Muthanna J. Ahmed

Department of Chemical Engineering, College of Engineering, University of Baghdad, Baghdad, Iraq

*** Corresponding author:** Aya B. Mohsin, aya.basit2307m@coeng.uobaghdad.edu.iq

ABSTRACT

Chitosan (CS) hydrogel beads were prepared by dropwise precipitation and surface-modified with three anionic surfactants—sodium dodecyl sulfonate (SDOS), sodium dodecyl sulfate (SDS), and sodium dodecylbenzene sulfonate (SDBS)—to improve methylene blue (MB) removal from water. FTIR and FE-SEM provided qualitative evidence of surface modification and increased surface roughness while indicating retention of the principal chitosan framework. The modified beads exhibited low BET surface areas (7.48–9.63 $m^2 g^{-1}$), and the surface-area order did not correspond to MB uptake, suggesting that surface chemistry and the accessibility of surfactant-derived anionic sites were more important than physical area alone. Triplicate batch experiments identified an optimum surfactant modification concentration of 3.0 g L^{-1} and an optimum solution pH of 6. Adsorption performance followed the order CS/SDOS > CS/SDS > CS/SDBS, with the highest experimentally achieved capacities of 418.60, 390.80, and 275.00 mg g^{-1}, respectively. Equilibrium was reached after approximately 240, 360, and 480 min, respectively. The pseudo-second-order model provided the best statistical description of the kinetic data ($R^2 \geq 0.995$), whereas the Sips model best represented the equilibrium data, indicating greater energetic heterogeneity for CS/SDOS and CS/SDS and near-Langmuir behavior for CS/SDBS. For CS/SDOS, MB removal decreased from approximately 95% for the fresh adsorbent to 52% after the first regeneration and 21% after the fifth regeneration with 0.1 M HCl, demonstrating limited reusability under the tested conditions. Future work should quantify surfactant loading and surface charge and evaluate milder regeneration media to improve adsorbent stability.

Keywords: methylene blue; anionic surfactant; surface modification; adsorption isotherm; kinetics

ARTICLE INFO

Received: 20 July 2026
Accepted: 31 August 2026
Available online: 15 September 2026

COPYRIGHT

Copyright © 2026 by author(s).
Applied Chemical Engineering is published by Arts and Science Press Pte. Ltd. This work is licensed under the Creative Commons Attribution-NonCommercial 4.0 International License (CC BY 4.0).
https://creativecommons.org/licenses/by/4.0/

1. Introduction

The global demand for freshwater has been greatly driven by the high population growth rate and industrial expansion, leading to a surge in water scarcity[1]. The quantity of wastewater produced has increased dramatically, resulting in an impact on the world's water resources and the introduction of pollutants (dye, heavy metals, organic compounds) in aquatic environments[2,3]. The textile sector is one of the main sources of this pollution, using approximately 350–380 m^3 of water to produce each ton of textile mass while releasing huge amounts of synthetic dyes[4]. Dyes are extensively used in the dye industry (plastic and textiles) uses dyes which include a "chromophore" group; this is what gives dyes their color[4]. Methylene Blue (MB) is an example of a cationic heterocyclic dye that is often used to represent the behavior of dye pollutants in water treatment[5]. This dye is discharged into surface waters with significant concern due to its persistence and ability to induce various negative health effects when large quantities are consumed (i.e., nausea, vomiting, cyanosis and methemoglobinemia)[6]. In order to tackle this critical environmental problem, several

wastewater treatment methods have been developed which include membrane filtration, ion exchange, oxidation, biodegradation, among others[7]. Of these processes, adsorption is one of the most popular choices because it is easy to use, costs less to run, and works well on diluted effluent. The mechanism relies on capturing dissolved contaminants from a fluid, binding them to a solid material's surface through either physical trapping or chemical bonds[8]. Increasingly, researchers have shown interest in modifying inexpensive by-products from agriculture and industry into potential adsorbent products[9]. Examples of promising adsorbents based upon biomass materials are coconut shell activated carbon[10] and modified agricultural fruit peel material[11]. Conventional adsorbents such as activated carbon have relatively high costs and regeneration challenges, and therefore, considerable research has been directed towards the use of low-cost biopolymers like chitosan, alginate, cellulose, and starch[12]. Chitosan is a promising biopolymeric adsorbent. The biopolymer is made from partially deacetylated chitin and consists of N-acetyl-D-glucosamine and D-glucosamine monomers that are connected with each other through a β-(1→4)-glycosidic bond. The abundant amino and hydroxyl groups in chitosan provide active sites capable of strong interactions with a wide variety of pollutants[13]. However, these benefits are offset by the low specific surface area, limited mechanical strength, and solubility in acidic solutions of pure chitosan. To overcome these limitations, chitosan composites and hydrogel have been chemically modified to enhance their sorption efficiency and structural stability[5]. Modification of those physic-chemical characteristics could be successfully carried out using surfactants as carriers, that is, through a process called surfactant assisted impregnation, where the anionic surfactant-molecules are held onto the hydrophilic networks of chitosan-beads, either by electrostatic or hydrophobic interactions and thus provide negatively charged head groups at the surface.

Anionic surfactant-sodium dodecyl sulfate (SDS) was used by[14], for modification of chitosan for the removal of Congo red (CR); while SDS gelled chitosan beads were used for methylene blue adsorption by[15]. While extensive research has been conducted on surfactant-modified adsorbents[9], few studies compared chitosan beads that had been modified with SDS, SDOS and SDBS; all three materials having been made and tested under identical test conditions. Therefore, it was unclear how the presence of sulfate head groups vs. sulfonate head groups would affect the adsorption capabilities of modified chitosan; nor was there clarity regarding the presence of an aromatic spacer. In recent years, there has been an expansion of adsorption/separation technology with the understanding that the ability to control the chemistry of a surface is necessary to develop effective mechanisms to remove pollutants. The literature contains numerous examples illustrating this, including: Adsorbent properties of nanopore lanthanum tungstate[16] and modified mesopore silica[17]; Modified Ion Exchange Membranes[18]; Hybrid Electro-Coagulation Adsorption Systems[19]; Functionalized membrane materials[19,20]A copper iron oxide/attapulgite composite material for MB removal (He, Gong et al., 2025); coal gasification slag-based adsorbents[21]; plant-derived nanofibrous membranes[22]; chlorite-based magnetic composite materials[23]; and magnetically responsive adsorbents formed through the alteration of kaolin using coal-series methods[24]. In combination, these studies demonstrate the importance of modifying surfaces; however, most were developed using inorganic/magnetic membrane-type technologies and therefore did not incorporate biodegradable chitosan. Photocatalytic-based dye-degradation technology has been shown to be an alternative process for wastewater treatment. These include photocatalysts such as polyoxometalate-based supported nanocomposite material, composite TiO_2, MoS_2 nanosheets, MnO_2 nanorods, and magnetic TiO_2 systems, which achieve very efficient removal of MB from water[25-30]. However, all of these are dependent upon a light source and catalyst recycling or intermediate-product removal considerations. Therefore, adsorption continues to offer many advantages in terms of providing a means of achieving both low-cost and low-energy separation. In addition, recent studies on waste-derived biosorbents have demonstrated their potential in removing MB from solution[31,32], with an emphasis on using renewable resources for the preparation of sorbents yet at the same time underlining the importance of having compatible charge interactions between modifiers and pollutants. The main novelty of the current paper is that it provides a systematic comparative analysis of SDS, SDOS, and SDBS with respect to modifying chitosan's. SDS and

SDOS have linear C_{12} hydrophobic chains; however, they differ by having sulfate or sulfonate functionalized head groups, while SDBS has a dodecyl hydrocarbon chain linked to a benzene ring and an end-functionalized sulfonate. Since SDS, SDOS, and SDBS were compared based on identical formulations and testing protocols, structural characteristics of the surfactants provide primary explanations for the observed differences. Because the amount of surfactant incorporated into chitosan film was determined indirectly, the relationship between the chemical structure of surfactants, the properties of surfaces produced from the incorporation of those surfactants into films, and their respective adsorption performance were treated in terms of possible mechanisms rather than established experimental facts. Therefore, the direct comparisons, along with assessments regarding limits of renderability of the tested materials represent contributions of this investigation. This research developed and evaluated chitosan beads, which were chemically modified with SDS, SDOS, and SDBS in accordance with the same experimental procedure. These materials were tested for their structural properties by FTIR spectroscopy, FE-SEM, and BET surface area measurements. In addition, their MB adsorption behavior has been studied as a function of the amount of surfactant used in their preparation, pH of the aqueous solution containing the adsorbate, initial dye concentration, and contact time. Experimental results have been interpreted according to pseudo-first-order and pseudo-second-order kinetics models and Langmuir, Freundlich, and Sips adsorption isotherm models. Finally, the reusability of the adsorbent that exhibited the highest adsorption capacity was investigated through a series of subsequent adsorption/desorption cycles.

2. Materials and methods

2.1. Materials

All of the chemicals that were employed throughout this research project were acquired directly from their respective suppliers. The chemical formula, purpose, purity or grade as provided by the supplier, and the name of each supplier are presented within **Table 1**. Chitosan (CS), Sodium Dodecyl Sulfate (SDS), Sodium Dodecyl Sulfonate (SDOS), and Sodium Dodecyl Benzene Sulfonate (SDBS) were selected due to their use as materials for the production of adsorbent materials. Acetic acid (glacial) was utilized to solubilize chitosan; however, methanol and NaOH were used to create a coagulation bath. HCl and NaOH were both employed for pH control, and HCl was also used as an eluent during regeneration. MB was chosen as the model cationic adsorbate. Distilled water produced on site at the laboratory was used as the source of distilled water for preparing all aqueous solutions.

Table 1. Chemicals used in the preparation of the adsorbents and adsorption experiments.

Material	Chemical formula	Purpose	Purity, grade, or relevant properties	Supplier
Chitosan (CS)	$(C_6H_{11}NO_4)_n$	Biopolymeric adsorbent	Medium molecular weight; average molecular weight 1,250,000 g mol^{-1}; viscosity 300-1000 cps; degree of deacetylation ≥90.0%	Glentham Life Sciences Ltd., Corsham, United Kingdom; product code GP8956
Methylene blue (MB)	$C_{16}H_{18}ClN_3S \cdot 3H_2O$	Model cationic adsorbate	Dye content ≥82%; certified by the Biological Stain Commission (BSC)	Sigma-Aldrich, St. Louis, MO, USA
Sodium dodecyl sulfate (SDS)	$C_{12}H_{25}NaO_4S$	Anionic surfactant modifier	99%	Glentham Life Sciences Ltd., Corsham, United Kingdom; product code GD2962
Sodium dodecyl sulfonate (SDOS)	$C_{12}H_{25}NaO_3S$	Anionic surfactant modifier	98%; analytical reagent grade	Sinopharm Chemical Reagent Co., Ltd., Shanghai, China
Sodium dodecylbenzene sulfonate (SDBS)	$C_{18}H_{29}NaO_3S$	Anionic surfactant modifier	Technical grade	Sigma-Aldrich (Merck KGaA), Darmstadt, Germany; product No. 289957

Glacial acetic acid	CH_3COOH	Solvent for dissolving chitosan	Minimum assay 99.5%	Alpha Chemika, India
Sodium hydroxide pellets	NaOH	Coagulation bath and pH adjustment	Minimum assay 98.0%; analytical reagent grade	SDFCL (Sd Fine-Chem Limited), Mumbai, India; product code 20252 K05
Hydrochloric acid	HCl	pH adjustment and regeneration eluent	35-38% w/w; relative density 1.18; analytical reagent grade	SDFCL (Sd Fine-Chem Limited), Mumbai, India
Methanol	CH_3OH	Component of the coagulation bath	Laboratory reagent grade; for synthesis	Thomas Baker Chemicals Pvt. Ltd., India; product No. 107726
Distilled water	H_2O	Preparation of all aqueous solutions	Distilled	Prepared in the laboratory

2.2. Instrumentation

To quantify the dye concentrations, we recorded the absorbance of the liquid samples with a Shimadzu UV-1900i UV-Vis spectrophotometer (Japan). Acidity levels were tracked via a Merck digital pH meter (Germany), which we standardized beforehand relying on pH 4.00 and 7.00 reference buffers. All chemical mixtures were homogenized atop a Genie magnetic stirrer (India), and the solid reagents were meticulously measured out on a Mettler Toledo analytical scale (India).

2.3. Characterization of beads

Fourier transform infrared spectroscopy (FTIR) was used to characterize the chemical functional group characteristics of the Hydrogel Beads made from the synthesized polymer. The spectra for each sample were taken on a Bruker vector 22 FTIR spectrometer (Bruker, Germany), via the Kbr pellet method. The spectra were collected from 400 – 4000 cm^{-1} wavenumbers. The surface morphology and microstructure of the dried hydrogel bead material were determined by field-emission scanning electron microscopy (FE-SEM) Surface textural properties of surfactant modified chitosan beads were determined using nitrogen adsorption/desorption isotherm measurements at 77k using a gas sorption analyzer (nano mavad saba; serial number 283). These measurements took place within the nano mavad Saba laboratory as per ISO 15901-2. Samples were air-dried under ambient conditions prior to being placed into vacuum at 120°C for 2 hours. The specific surface area (s bet) was calculated using the Braeuer-Emmet-Teller method over an approximate relative pressure range of 0.01 to 0.23 with linear fitting correlation coefficients of ≥ 0.995. Total pore volume was estimated at p/po = 0.99 and average pore diameter was calculated from the s bet and total pore volume values.

2.4. Synthesis of chitosan (CS) hydrogel beads

Chitosan hydrogel beads were prepared using a modified version of the precipitation technique originally presented by[33]. In brief, 3 grams of chitosan powder were mixed under continuous agitation overnight while dissolved in 250 ml of a 7% (v/v) aqueous solution of acetic acid to form a homogenous, viscous solution. This solution was then added dropwise, at an average rate of 40-50 drops/minute, using a pipette into a preformed alkaline coagulating solution that consisted of distilled water, methanol, and sodium hydroxide at a weight ratio of 4:5:1 (w/w/w), respectively. Immediately upon contact with the coagulant, each drop formed into a spherical hydrogel bead. Wet beads were left in this coagulant for approximately 6 hours to allow for gelation. After the beads had completed the gelation process, they were rinsed multiple times with distilled water to remove any remaining residual alkalinity; once the pH of the rinse water was around 7.0, the beads were removed from the rinse water. Beads were next passed through a sieve to obtain a size range of 0.6-1.0 mm and stored in distilled water until further use. The basic steps involved in preparing the beads are illustrated graphically in **Figure 1**.



Figure 1. Schematic illustration of the preparation of surfactant- loaded chitosan composite beads.

2.5. Modification of CS beads by surfactants

Chitosan beads that had been recently synthesized were subjected to individual surface modification by use of either sodium dodecyl sulfate (SDS), sodium dodecyl sulfonate (SDOS), or sodium dodecylbenzene sulfonate (SDBS) as anionic surfactants. In this way, for every surface modification study, 500 fresh chitosan beads were placed into 100 mL of aqueous surfactant solutions that ranged from 500 to 5000 mg/L. Each of the surfactant solutions was made to have a pH of 6. Each bead-surfactant system was then left stationary at approximately room temperature (25°C) for five days[33]. Afterward, the modified beads were removed from their respective surfactant solutions and dried at ambient conditions for six hours. In order to select the appropriate number of beads per sample based upon prior experimentation, the previously reported optimization results are discussed in detail within Section 3.2. As such, all subsequent adsorption studies will be conducted using beads that have undergone modification via application of a surfactant concentration of 3000 mg/L. Accordingly, these resultant products will be denoted as CS/SDS, CS/SDOS, and CS/SDBS, respectively, in accordance with the surfactant used during the initial modification step.

2.6. Batch adsorption experiments

The adsorption of methylene blue (MB) onto surfactant-modified chitosan hydrogel beads (CS/SDOS, CS/SDS, and CS/SDBS) and unmodified chitosan hydrogel beads was studied. Prior to the experimentation with the beads, they had been dried using air at room temperature for 6 hr. A dry adsorbent mass of 0.02g was added to 40 mL of MB solution with a known initial concentration.

Each adsorption study was conducted under static conditions (no agitation) at ambient laboratory temperature (25 °C). A deliberate decision was made to avoid agitation because the anionic surfactants produced significant amounts of foam. Agitation created turbulence that allowed air to enter the system, also creating a concentration gradient for both the surfactant and dye in relation to the liquid surface; this may have disturbed the adsorption equilibrium, causing inaccurate readings of the residual concentrations.

To replace mechanical stirring, extended contact times of 24 hours were utilized for all adsorption studies; this extended contact time was confirmed by the kinetic study (Section 3.5) to be greater than sufficient to achieve equilibrium.

Chitosan hydrogel beads were modified with surfactants SDOS, SDS and SDBS at varying concentrations; 0.5, 1,5, 3 and 5 L^{-1}. The effect of surfactant concentration was evaluated at 25°C using 100 mg L^{-1} MB at pH 6 for 24hr. To determine the impact of the solution's pH on the adsorption process, the pH was adjusted using dilute HCl or NaOH. The pH study was performed at pH 2, 4, 6, 8, 10, and 12 using an initial MB concentration of 100 mg L^{-1}. Adsorption equilibrium experiments were conducted over an initial MB concentration range from 50 to 550 milligrams per liter at room temperature (25 °C) and pH 6. These experiments were allowed to proceed for 24 hours so that equilibrium could be reached. The hydrogel beads containing the optimal amount of surfactant (3g L^{-1}), based upon the previous optimization study, were used in all subsequent adsorption experiments. Kinetic studies were run using an initial MB concentration of 100 milligrams per liter and contact times extended to 1440 min. Unless otherwise stated, all adsorption experiments used a 24 h contact time. After each experiment, the beads were separated from the solution by filtration, After completion of each adsorption experiment, the remaining MB concentration in solution was determined by measuring absorbance at the maximum wavelength of absorbance (λmax = 665 nanometers) using a UV-Vis Spectrophotometer. Using a previously developed calibration curve. All adsorption experiments were conducted in triplicate, and the results are reported as the mean ± standard deviation. Finally, the mass balance formula was applied to determine the equilibrium adsorption capacity (q_e, expressed in mg g^{-1})[33]:

$$q = \frac{(C_0 - C_e)V}{w} \quad (1)$$

Where C_o (mg L^{-1}) is the initial dye concentration, C_e (mg L^{-1}) is the equilibrium dye concentration, V (L) is the solution of volume and W (g), is the dry mass of adsorbent.

2.7. Adsorption isotherm models

Adsorption isotherms studies were performed to describe the interaction between methylene blue molecules and the surface of CS/SDOS, CS/SDS, CS/SDBS hydrogel beads under equilibrium conditions. Experiments were conducted at a constant temperature of 25 °C and pH 6, using initial MB concentration ranging from 50 to 550 mg L^{-1}. The equilibrium time required for adsorption was approximately 24 hr. The experimental data were analyzed using three commonly applied isotherm models, namely the Langmuir, Freundlich, and Sips isotherm models. These models were used to interpret the adsorption mechanism and determine the best-fitting models based on statistical parameters such as the correlation coefficient (R^2) and chi-square (X^2). The Langmuir isotherm assumes monolayer adsorption onto a homogeneous surface with a finite number of identical active sites. The Langmuir isotherm model can be expressed as follows[34]:

$$q_e = \frac{q_m k_L C_e}{1 + k_L C_e} \quad (2)$$

where C_e (mg L^{-1}) represents the equilibrium concentration of the adsorbate, q_e (mg g^{-1}) is the adsorption capacity at equilibrium, the parameter q_m (mg g^{-1}) represents the maximum monolayer adsorption capacity, while K_L (L mg^{-1}) is the Langmuir constant associated with the affinity between the adsorbent surface and methylene blue molecules[35]. The Freundlich isotherm model is given by[34]

$$q_e = K_F C_e^{\frac{1}{n}} \quad (3)$$

where q_e (mg g^{-1}) is the equilibrium adsorption capacity, C_e (mg L^{-1}) reflects the residual MB concentration remaining in the liquid phase. Furthermore, K_F is the Freundlich coefficient linked to the overall binding capacity, and n serves as the heterogeneity index, which points to the structural unevenness of the material's surface.

Building on this, the equation for the Sips isotherm model is expressed as follows[36]:

$$q_e = \frac{qK_{eq}C_e^n}{1 + K_{eq}C_e^n} \quad (4)$$

Where q_e (mg g^{-1}) is the equilibrium adsorption capacity, C_e (mg L^{-1}) is the equilibrium concentration, q_{max} (mg g^{-1}) represents the maximum adsorption capacity, K_{eq} (L mg^{-1}) is the Sips equilibrium constant, and n describes the heterogeneity of the adsorption system. When $n_s = 1$, the Sips equation reduces to the Langmuir equation. At low equilibrium concentrations, it approaches Freundlich-type behavior, whereas at high concentrations it predicts a finite monolayer capacity similar to the Langmuir model.

2.8. Regeneration and reusability

The reusable properties of the chitosan impregnated with a surfactant were evaluated using five repeated adsorption/desorption cycles. In all cases, the dye loaded adsorbent was separated from the dye-laden solution via filtration after the adsorption process. Then the dye-laden adsorbent was placed into 40 mL of 0.1M HCl and stirred at room temperature for 60 minutes at 500 rpm. This acidic environment causes the active site on the surface of the adsorbent to be protonated and thus weaken the electrostatic interaction between the adsorbent and the cationic dye[37]. Following this procedure, the regenerated adsorbent was again subjected to filtration, rinsed with distilled water until neutral, air-dried at room temperature for 6hr, and used in subsequent cycles.

For all adsorption procedures, all parameters were optimized based on previous studies (adsorbent dosage: 0.02 g/40 ml solution; dye concentration: 100 mg L^{-1}, Temperature: 25°C, pH 6; contact time: 24 h; static condition). Additionally, residual dye concentrations were determined after each cycle. The removal efficiencies were compared to those obtained during the first cycle. All regeneration experiments were conducted in triplicate, and the results are reported as the mean ± standard deviation The percent desorption was calculated as follows:

$$DP\% = \frac{C_d}{C_{ad}} \quad (5)$$

where C_d is the quantity of dye removed during desorption, $C_{ad}=C_i-C_e$ is the quantity of dye adsorbed where C_i and Ce are respectively the concentrations of dye at time zero and at equilibrium (in mg L^{-1}).

3. Results and discussion

3.1. Preparation and gelation mechanism of CS hydrogel beads via alkali treatment

The chitosan solution droplets were neutralized in an alkaline medium to form chitosan hydrogel beads. In this process, the protonated amine groups ($–NH_3^+$) of chitosan were converted to deprotonated amine groups ($–NH_2$), resulting in a decrease in electrostatic repulsion between polymer chains[38]. As a result, polymer aggregation occurred leading to the formation of stable hydrogel beads. Physical crosslinking is proposed as the main crosslinked mechanism for the formed hydrogel, while intermolecular interactions, including hydrogen bonding and chain entanglement, may contribute to the formation of a three-dimensional network structure. Furthermore, the balance between hydrophilic and hydrophobic interaction within chitosan matrix affects the gelation behavior[14]. This balance contributes to the structural integrity and mechanical strength of the hydrogel beads. previous studies have reported similar observations, supporting the significance of intermolecular forces in chitosan gelation systems.

3.2. Effect of anionic surfactant concentration on cationic dye (MB) adsorption

Figure 2 shows the effect of the surfactants modification concentration (0-5g L^{-1}) on MB adsorption. The amount of dye adsorbed by the modified adsorbent using anionic surfactants was higher than that adsorbed by the unmodified adsorbent. This may be associated with an increased presence of negatively charged anionic surfactant species on the adsorbent surface, thereby increasing the negative surface charge density and

potentially enhancing electrostatic attraction towards positively charged MB. However, since surfactant loading and surface charge were not measured experimentally, an explanation of this type is offered here as a mechanistic interpretation rather than experimental verification. For SDOS and SDS, the adsorption capacity increased up to a modification concentration of 3g L^{-1} and decreased slightly at 0.5 g L^{-1} The decline in adsorption capacity may have been due to surfactant monomer aggregation at high surfactant loadings (which would diminish available monomers and/or occlude access to pores); however, neither CMC nor aggregation experiments were conducted during this study. Therefore, all subsequent experiments utilized a modification concentration of 3 g $L^{-1.}$ For the SDBS modified adsorbent The increase in adsorption capacity was smaller than that seen for both SDOS and SDS and, like them, achieved a maximum at 3.0 g L^{-1}. The relatively smaller effect may result from steric hindrance produced by the benzene ring and the lower CMC value of SDBS; however, this too is speculative, as there are no quantitative data on surfactant loading. This observation is also consistent with the kinetic data where SDBS-modified adsorbent had both the lowest dye removal capacity and slowest initial adsorption rate (Das & Pal, 2016).Data are presented as mean ± standard deviation (n=3).

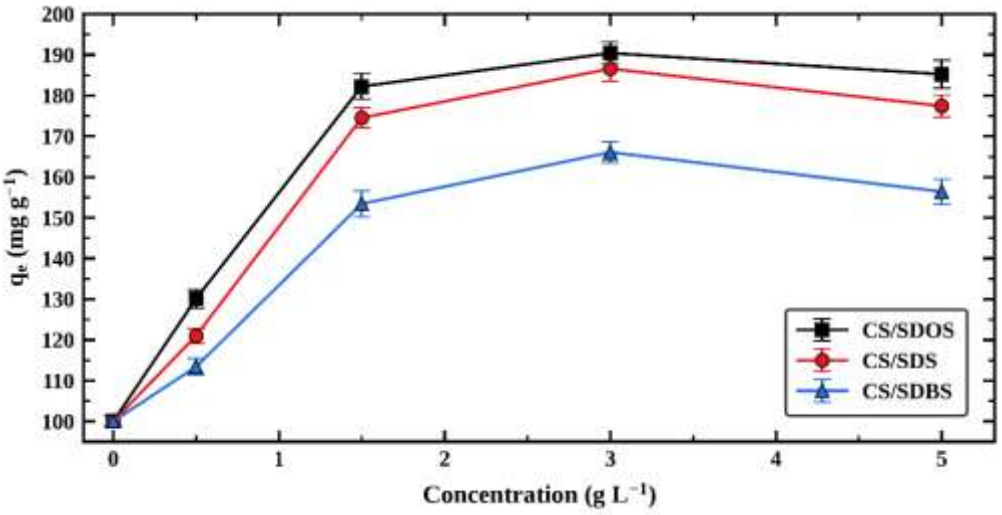


Figure 2. Effect of concentration on the adsorption capacity (q_e) of hydrogel beads for methylene blue removal.

3.3. Characterization

3.3.1. Surface morphology characterization (FE-SEM)

The FE-SEM images of the untreated and surfactant- modified chitosan beads are presented in **Figure 3**. (I) CS, (II) CS/SDBS, (III) CS/SDOS, (IV) CS/ SDS). The untreated CS sample exhibited a relatively smooth and compact surface with a limited number of surface irregularities. In comparison, the surfactant-modified samples exhibited more heterogeneous and roughened surface morphologies. The CS/SDBS sample displayed dense, cauliflower-like aggregates, whereas the CS/SDOS and CS/SDS showed irregular, folded, and relatively fine-grained surface feature. The structural differences seen in the FE-SEM images are consistent with changes that occur post-surfactant. However, the FE-SEM images themselves do not provide quantitative measurements of how much surfactant is being loaded on the surfaces or how well those surfaces are covered. Thus, the observed structural differences are considered indirect evidence for surface modifications vs. the actual amount and/or arrangement of surfactants on the surfaces. The uneven morphologies of CS/SDOS and CS/SDS will likely result in a greater number of heterogeneities at the adsorbent/solution boundary and therefore can account for their ability to bind more MB. Conversely, the large aggregates seen in CS/SDBS may limit access to certain adsorption sites, resulting in less MB being bound. Mechanistically, this finding represents interpretations since there was no measurement made regarding how much surfactant was actually loaded onto each sample's surface and how accessible the adsorption sites were[39]

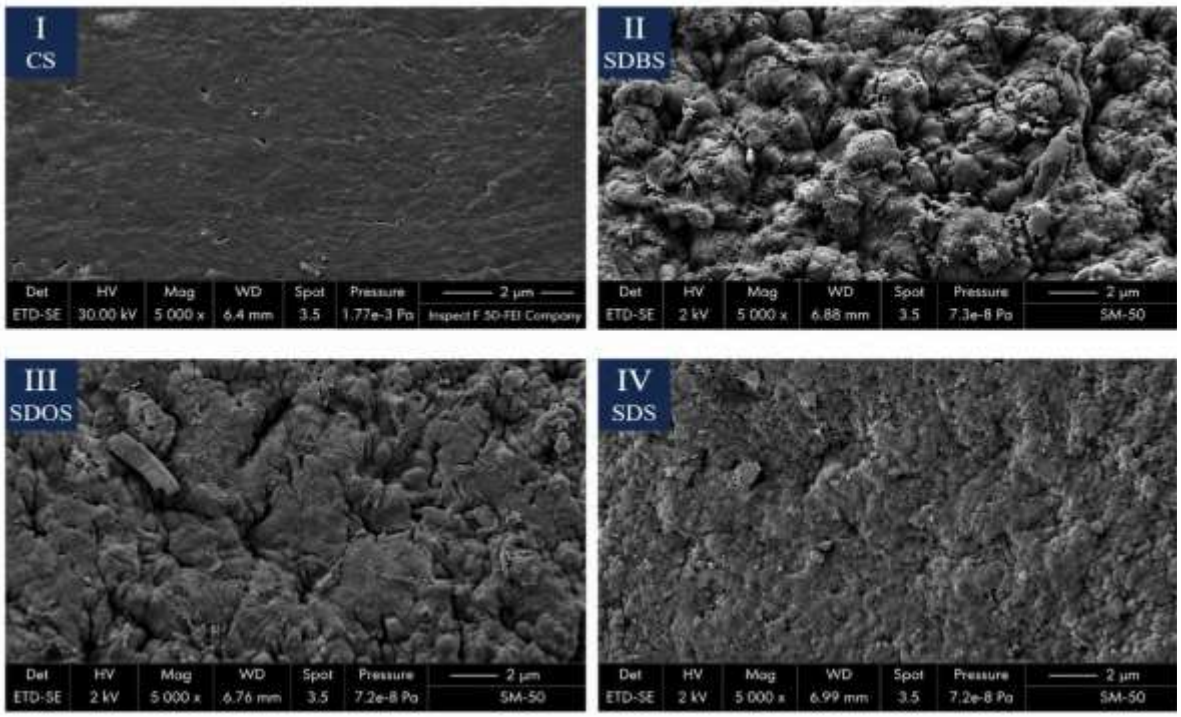


Figure 3. FE-SEM micrographs of (I) CS, (II) CS/SDBS, (III)CS/ SDOS and (IV)CS/ SDS.

3.3.2. FTIR analysis

FTIR spectra for unmodified (CS) and surfactant-modified adsorbents (CS/SDOS, CS/SDBS, CS/SDS) are presented in **Figure 4**, and the principal band assignments are summarized in **Table 2**. There were some similarities among the four infrared spectra, as each retained the majority of the characteristic absorption bands of the chitosan backbone. Some minor changes were noted along with the addition of several absorption bands attributed to the presence of the surfactant. These observations suggest that while the basic structure of the chitosan backbone remains largely unchanged after modification, there are likely to be alterations in the local chemical environment surrounding the polymers due to interactions between the surfactant(s) and chitosan. A broad band observed at approximately 3400-3500 cm^{-1} is assigned to Overlapping N-H (amide) and O-H (hydrogen-bonding) stretching bands, with contribution from surface hydroxyls and adsorbed water. Absorption in the frequency range of 1637-1653 cm^-1 corresponds to a combination of N-H bending and O-H bending from absorbed water. While the shifts seen for this area can indicate changes in the extent of hydrogen bonding and/or interaction of the surfactant with the chitosan, they do not provide quantitative information about how much of the surfactant has been loaded onto the chitosan. A very weak peak seen at 2891 cm^{-1} (CS) is due to CH stretch from alkane C-H bonds. Peaks seen between 1460-1300 cm^{-1} are due to bending deformation of C-H bonds. in CS/SDS, the bands at 1460 and 1375 cm^{-1} correspond to CH_2 deformation of the dodecyl chain. The strong absorption in the 1000-1150 cm^{-1} range is associated with C-O-C and C-O stretch frequencies for the polysaccharide backbone. This region overlaps with frequencies of the head groups of both SDS and SDOS when those surfactants have reacted with CS. A band at 1113 cm^{-1} for CS/SDS is assigned to an S = O stretch in the sulfate ester group ($-OSO_3^-$). Similarly, a band at 1084 cm^{-1} for CS / SDOS is assigned to vibrations from sulfonate groups. In addition, two bands at 1221 and 1148 cm^-1 in CS/SDBS are assigned to asymmetric and symmetric S = O stretches. Additionally, CS/SDBS shows bands at 835, 746, and 698 cm^{-1} indicative of aromatic C-H out-of-plane bending around a benzene ring present in SDBS. As expected, the bands present in the surfactant-related regions support the presence of respective functional groups within modified samples. The observation of bands associated with the surfactant interacting with chitosan indicates that the incorporation of the surfactant into chitosan has taken place. However, based

upon retention of the major bands present for chitosan, it appears that no significant disruption occurred to the backbone during modification. Thus, while FTIR demonstrates qualitatively that modification occurred and supports interaction between surfactant(s) and chitosan, it cannot quantify either the amount of surfactant incorporated or the surface density of such modifications.

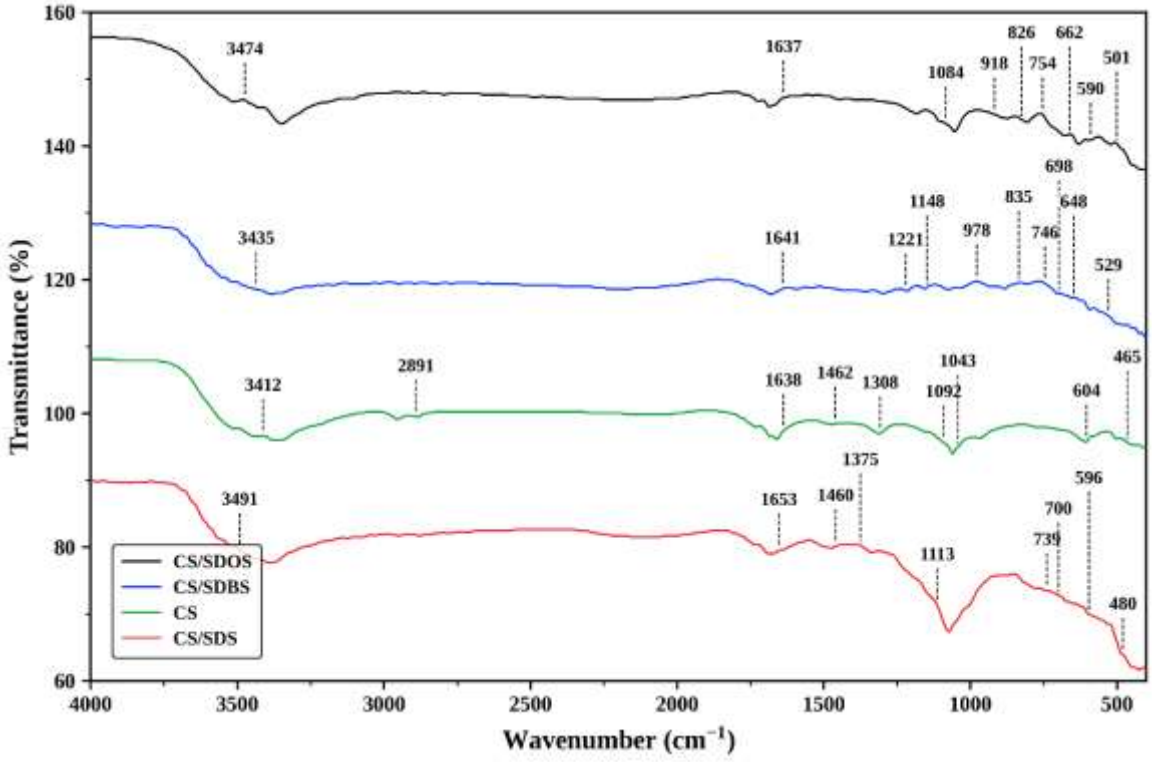


Figure 4. FTIR spectra of CS, CS/SDOS, CS/SDBS, CS/SDS.

Table 2. Principal FTIR band assignments (cm^{-1}) for chitosan and the surfactant-modified beads.

Assignment	CS	CS/SDOS	CS/SDBS	CS/SDS
O–H / N–H stretch	3412	3474	3435	3491
C–H stretch (alkyl)	2891	–	–	–
Amide I / N–H bend (+ H–O–H)	1637, 1616	1637, 1616	1641	1653
CH_2 scissor / bend (tail)	1462, 1307	–	–	1460, 1375
S=O asymmetric. (sulfonate)	–	–	1221	–
S=O symmetric. (sulfonate)	–	1084.0	1148	–
S=O (sulfate ester)	–	–	–	1113
Aromatic ring C–H (out-of-plane)	–	–	835, 746, 698	–
C–O–C / C–O (backbone)	1091.7, 1043.5	1091, 1043	overlapped	overlapped

3.3.3. BET analysis

The textural properties of the three surfactant-modified beads, obtained from N_2 adsorption at 77 K, are summarized in **Table 3**, and the isotherms are shown in **Figure 5**. All three adsorbents exhibited low BET specific surface areas, in the order CS/SDS (9.63 $m^2\ g^{-1}$) > CS/SDOS (7.84 $m^2\ g^{-1}$) > CS/SDBS (7.48 $m^2\ g^{-1}$),

consistent with the dense, low-porosity nature of chitosan hydrogel beads. The nitrogen isotherms for CS/SDS and CS/SDOS show that as pressure increases, more nitrogen is adsorbed, with very little difference when the pressure is decreased. This type of adsorption behavior indicates that both samples have surfaces primarily consisting of either non-porous or microporous areas with Type II isotherm characteristics. On the other hand, CS/SDBS exhibits rapid increases in adsorption near saturation and a large H3-type hysteresis loop. It can be inferred that this sample has a relatively higher total pore volume (i.e., 0.141 $cm^3\ g^{-1}$) and a larger mean pore diameter (i.e., 75.4 nm). Consequently, the significant pore volume and pore size may be due to the presence of void spaces between particles, as well as larger slit-shaped pores. Therefore, it is unlikely that the majority of the adsorption sites are located at micropores on the surface of these particles. The BET C constant could not be determined for this sample. Notably, the BET surface-area order does not match the MB adsorption order (CS/SDOS > CS/SDS > CS/SDBS): the highest-area sample (CS/SDS) did not the best adsorbent, and the largest-pore-volume sample (CS/SDBS) is the poorest. Results from this study also demonstrate that physical surface area and/or pore volume do not dictate adsorption of methylene blue onto the surfactant-modified chitosan's. However, it appears that surface chemistry and the interaction(s) occurring between methylene blue and the modified chitosan most likely contribute significantly to adsorption. However, the contributions of surfactant loading, anionic group density, and site accessibility could not be quantified because these parameters were evaluated qualitatively.

Table 3. Textural properties of the surfactant-modified chitosan adsorbents from N_2 adsorption at 77 K.

Sample	V_m (cm^3 STP g^{-1})	S_{BET} ($m^2\ g^{-1}$)	BET C	Corr. Coeff.	Total pore vol. ($cm^3\ g^{-1}$)	Avg. pore dia. (nm)
CS/SDS	2.2137	9.6349	108.46	0.9995	0.008004	3.3229
CS/SDOS	1.8008	7.8379	75.62	0.9988	0.007918	4.041
CS/SDBS	1.7175	7.4756	—	0.9954	0.1409	75.416

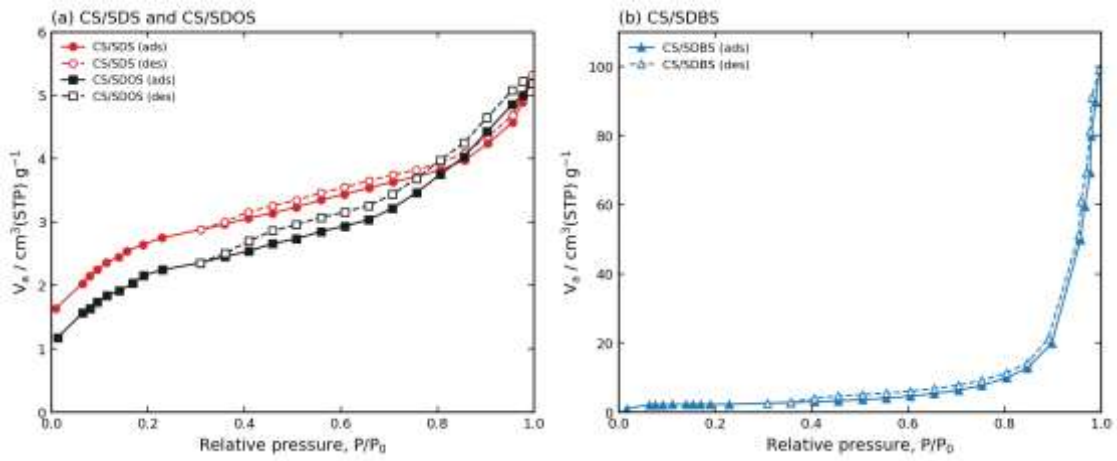


Figure 5. N_2 adsorption–desorption isotherms at 77 K: (a) CS/SDS and CS/SDOS (b) CS/SDBS Filled symbols represent adsorption, and open symbols represent desorption.

3.4. Effect of pH

The effect of the initial solutions of pH on MB adsorption by the three surfactant-modified adsorbent was evaluated over the pH range 2 – 12. The results are presented in **Figure 6** as (a) adsorption capacity, q_e, and (b) removal efficiency. Both q_e and removal efficiency increased for all three adsorbents as the pH level increased from 2 to 6. reached maximum value at pH 6, and subsequently decreased up to pH 12. In terms of adsorption performance, there are similarities among all three adsorbents; specifically, as the pH level changed, each adsorbent followed an order that included CS/SDOS > CS/SDS > CS/SDBS. Data collected in previous

experiments also supports the above-described trend of adsorption. Therefore, pH = 6 was used for additional studies. Removal efficiency was determined using adsorption capacity, while the standard deviation for removal efficiency was determined based on the previously reported standard deviation for q_e. One reason why pH could impact adsorption performance could be due to electrostatic interaction among positively charged MB molecules and those functional groups found on the chitosan bead modified with SDS. When pH is lower than 7, it is likely that there will be enough H^+ present in solution to compete for available adsorption sites. Moreover, when these H^+ ions interact with the functional group on the surface of the bead, they can cause them to become protonated, which reduces the number of negatively charged sites available to bind MB and thus would reduce the electrostatic attraction between MB and the bead and result in reduced adsorption[40].Another potential reason why pH may affect adsorption performance is that as the pH of the solution increases, the functional groups on the surface of the bead become more deprotonated. Deprotonation of functional groups on the surface of the bead would lead to an increase in the number of negatively charged binding sites, which would lead to an increase in electrostatic attraction between MB and the bead and ultimately lead to an increase in adsorption until pH=6. However, beyond pH=6, the decreased adsorption rates may be related to changes in surface speciation, the nature of interactions between the adsorbent and adsorbate, and/or structural changes within the modified chitosan bead. Additionally, partial desorption of surfactants into solution at highly basic conditions could potentially explain the loss of adsorption capability[41] , although direct measurement of surfactant leachate during this experiment was not performed. Although the three altered adsorbent materials had differing amounts of MB adsorbed onto their surfaces, both the CS/SDOS, as well as the CS/SDS material, demonstrated greater MB adsorption performance over that of the CS/SDBS. These trends are consistent with the previous adsorption and morphological analyses. However, due to the lack of quantitative measurements for such variables as surfactant surface area coverage, anionic group concentration, and accessibility of adsorption sites; there was no direct evidence provided to quantify differences in those properties.

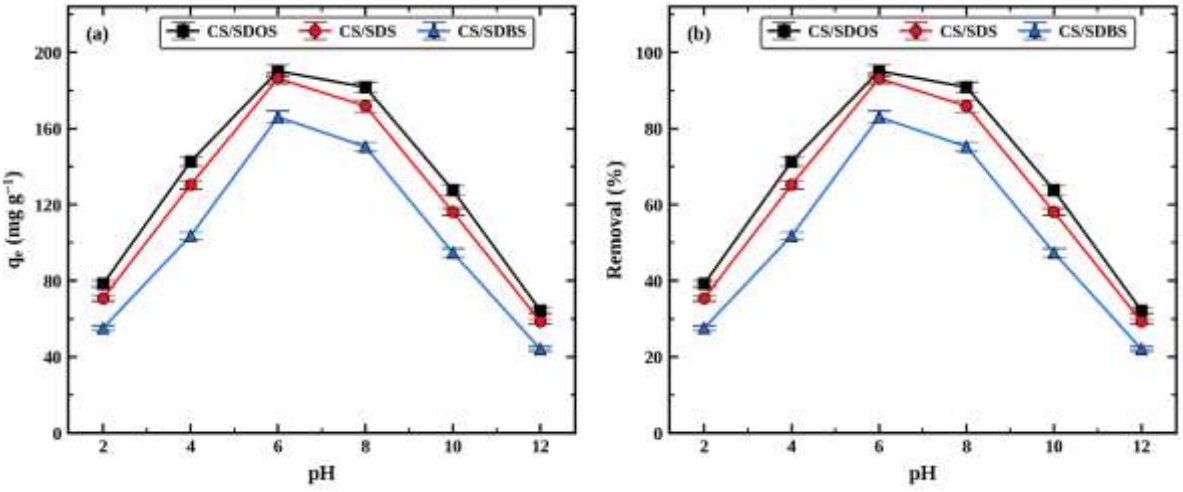


Figure 6. Effect of initial pH of MB solution on adsorption by surfactant-modified beads. (a) adsorption capacity and (b) removal efficiency. Data are presented as mean mean ± SD (n = 3).

3.5. Kinetic study

Contact time greatly influenced the sorption of methylene blue (MB) onto the adsorbent modified with sodium dodecyl sulfonate (SDOS), sodium dodecyl sulfate (SDS) and sodium dodecyl benzene sulfonate (SDBS). The three adsorbents showed a fast initial phase of adsorption where about 83% (CS/SDOS), 73 % (CS/SDS) and 62 % (CS/SDBS) of the equilibrium capacity was achieved during the first 60 minutes. These high initial uptakes can be attributed to the large number of vacant surface sites and steep concentration gradient present at the beginning of the experiment. Each kinetic experiment was performed in triplicate, and

the results are expressed as mean ± SD (n = 3). After the surface sites have been filled to a greater extent, the adsorption rate slows down and stabilizes, with the equilibrium being attained around 240 min for CS/SDOS, 360 min for CS/SDS and 480 min for CS/SDBS. For all subsequent experiments, a contact time of 1440 min was chosen to allow the completion of equilibration of all systems. Based upon the equilibrium capacities shown in **Table 4**, the experimental equilibrium capacities are in the same order as CS/SDOS>CS/SDS>CS/SDBS. It is worth noting that at C_o=100 mg/L (V=40 mL, m=0.02g), the theoretical maximum capacity based on mass balance for removal of MB into the solid is 200mg/g. Therefore, under conditions close to exhaustion, CS/SDOS and CS/SDS can remove approximately 95% and 93%, respectively, of the MB from solution. At such nearly exhaustive levels of uptake, kinetic experiments will primarily distinguish between the adsorption rates of the two highest performing materials rather than their ultimate capacities that are better defined through isotherm studies. The kinetic data were also analyzed using non-linear regression using Origin software according to the original, non-linearized forms of the pseudo-first-order (PFO) and pseudo-second-order (PSO) models presented as follows:

$$\boldsymbol{q_t = q_e(1 - e^{-k1t})} \quad \textbf{(6)}$$

$$\boldsymbol{\frac{t}{q_t} = \frac{1}{K_2 q_e^2} + \frac{t}{q_e}} \quad \textbf{(7)}$$

The terms q_t (mg g^{-1}), where t (min) is the adsorption time, q_e (mg g^{-1}), where this is the predicted adsorption capacity for the model at equilibrium, k_1 (min^{-1}), where the first term refers to the rate constant for the PFO step; and k_2 (g mg^{-1} min^{-1}), where the second term describes the rate constant for the PSO step, are each parameters in the PSO equation given in Eq.6. The fitted parameters and errors are summarized in **Table 4**. Although the PFO model had satisfactory fits to the data, it consistently produced smaller equilibrium capacities than were measured, especially when ($q_e - q_t$) was close to 0. For each of the three adsorbents, the PSO model provided the best statistical representation based on its larger R^2 values, smaller RMSE and χ^2 values, and closest agreement between the calculated and experimentally determined capacity (q_e,cal vs. q_e,exp). Additionally, the modeled capacities did not exceed the limits established from the experimental mass balance. While the improved fit of the PSO model represents an empirical description of the kinetic data, it cannot alone indicate that a chemisorption reaction has occurred. However, the observed kinetic behavior is compatible with both the impact of available sites for adsorption and electrostatic interaction between the positively charged MB molecules and the negative charge due to the presence of sulfonate or sulfate groups present on the surfactant molecule, which are supported by both pH measurements and FTIR analysis. Both the PSO adsorption rate parameter ($h = k_2 q_e^2$) and k_2 for each of the three surfactants follow the same order as those experimentally measured for achieving equilibrium, i.e., CS/SDOS > CS/SDS > CS/SDBS.

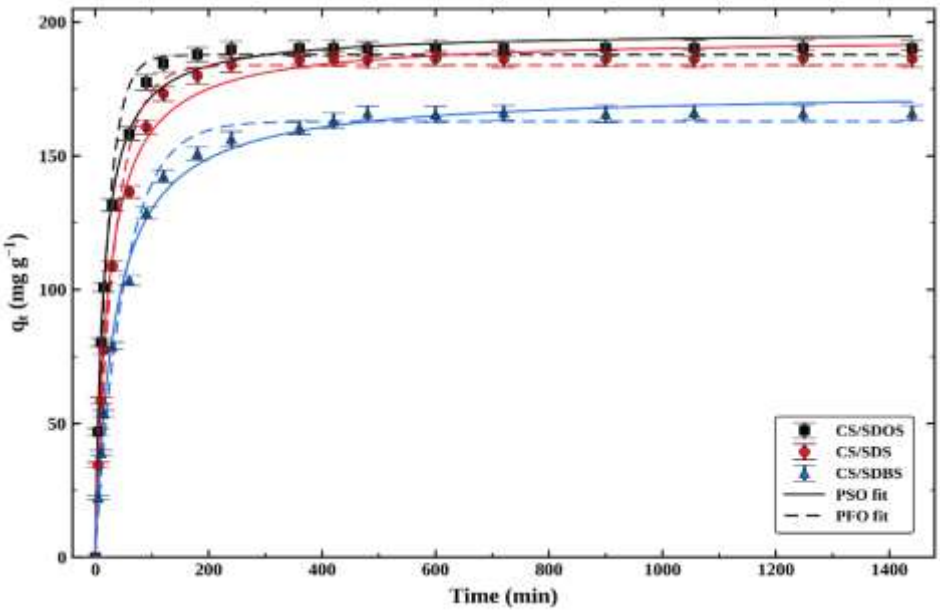


Figure 7. Adsorption kinetics of MB on surfactant-modified chitosan beads. Symbols represent mean ± SD (n = 3); solid and dashed lines represent nonlinear PSO and PFO fits, respectively. Conditions: C_0 = 100 mg L^{-1}, adsorbent dose = 0.02 g/40 mL, surfactant modification concentration = 3.0 g L^{-1}, pH 6, 25 °C, and no agitation.

Table 4. Nonlinear kinetic-model parameters for MB adsorption on surfactant-modified chitosan beads.

Model	Parameter	CS/SDOS	CS/SDS	CS/SDBS
Experimental	$q_{e,exp}$ (mg/g)	190.20	186.30	166.04
Pseudo-first-order	$q_{e,cal}$ (mg/g)	187.74	183.88	162.90
	k_1 (min^{-1})	0.0465	0.0295	0.0195
	R^2	0.9873	0.9877	0.9887
	RMSE (mg/g)	6.31	6.52	5.84
	χ^2	6.89	11.18	13.56
Pseudo-second-order	$q_{e,cal}$ (mg/g)	196.51	194.36	174.32
	k_2 (g mg^{-1} min^{-1})	3.63×10^{-4}	2.34×10^{-4}	1.69×10^{-4}
	h (mg g^{-1} min^{-1})	14.00	8.82	5.14
	R^2	0.9954	0.9950	0.9964
	RMSE (mg/g)	3.80	4.15	3.31
	χ^2	1.84	2.05	1.58

3.6. Isotherm study

A comparison of the Adsorption isotherms of methylene blue. Isotherm analysis of the equilibrium data collected at 50 – 550 mg/L methylene blue, at equilibrium, has been carried out using the Langmuir, Freundlich and Sips isotherm models **Figure 8**. The experiments were done three times. Therefore, the plotted data is expressed as the average of those trials ± standard deviation (n=3). The parameters were found via non-linear regression of the original model equations using Origin to fit 8 different concentration points for each equation. The fitted n_s values for CS/SDOS (0.518) and CS/SDS (0.629) indicate appreciable energetic heterogeneity toward MB, explaining why the flexible Sips equation described these datasets better than the single-energy Langmuir model. However, the Sips capacities predicted for CS/SDOS (507.62 mg g^{-1}) and CS/SDS (445.03

mg g^{-1}) exceed the highest experimentally achieved adsorption capacities (418.60 and 390.80 mg g^{-1}, respectively) and therefore involve extrapolation beyond the measured adsorption range. These fitted q_{max} values should consequently be interpreted as model estimates rather than directly measured capacities. The lower Langmuir capacity obtained for CS/SDOS reflects the continued gradual increase in uptake over the measured range rather than a sharply defined plateau. In contrast, the n_s value for CS/SDBS (1.158) is relatively close to unity; accordingly, the Langmuir and Sips models produced similar fits and comparable capacity estimates for this adsorbent.

The Freundlich model does not impose a finite saturation capacity and was therefore less able to describe the onset of the plateau, particularly for CS/SDBS. Across the three adsorbents, the fitted capacity followed the order CS/SDOS > CS/SDS > CS/SDBS. The Sips affinity parameter showed the same order. Within the fitted Sips model, this trend indicates a higher apparent affinity for CS/SDOS; however, the fitted constant should not be interpreted as a direct measurement of bond strength.

Overall, the equilibrium data are consistent with MB adsorption on a finite population of energetically non-equivalent sites, particularly for CS/SDOS and CS/SDS. The proposed relationship between adsorption performance and the density or accessibility of anionic sites is a mechanistic interpretation because surfactant loading and surface-site density were not quantified directly. The different isotherm behaviors may therefore reflect differences in surfactant organization and in the resulting distributions of accessible binding-site energies on the chitosan surface.

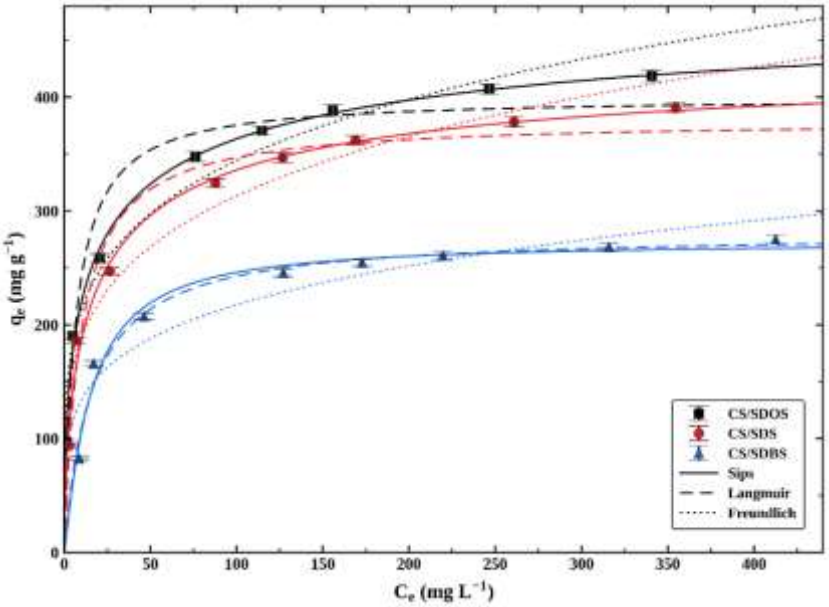


Figure 8. Equilibrium adsorption isotherms of MB on surfactant-modified chitosan beads. Symbols represent mean ± SD (n = 3); solid, dashed, and dotted lines represent nonlinear Sips, Langmuir, and Freundlich fits, respectively. Conditions: initial MB concentration = 50–550 mg L^{-1}, adsorbent dose = 0.02 g/40 mL, surfactant modification concentration = 3.0 g L^{-1}, pH 6, 25 °C, 24 h, and no agitation.

Table 5. Isotherm parameters for methylene blue adsorption onto surfactant-modified chitosan adsorbents.

Adsorbent	Model	q_{max} (mg/g)	Constant	n, n_s	R^2	RMSE	χ^2
CS/SDOS	Langmuir	400.06	K_L = 0.1522	—	0.9485	24.68	27.58
	Freundlich	—	K_F = 131.50	n = 4.784	0.9626	21.04	17.48
	Sips	**507.62**	**K_s = 0.2315**	**n_s = 0.518**	**0.9959**	**6.97**	**2.34**
CS/SDS	Langmuir	380.03	K_L = 0.1049	—	0.9652	18.48	11.14
	Freundlich	—	K_F = 112.35	n = 4.490	0.9449	23.26	23.22

	Sips	**445.03**	**K_s = 0.1699**	**n_s = 0.629**	**0.9868**	**11.39**	**7.16**
CS/SDBS	Langmuir	280.74	K_L = 0.0638	—	0.9752	9.78	6.06
	Freundlich	—	K_F = 82.27	n = 4.736	0.8751	21.94	24.99
	Sips	**273.02**	**K_s = 0.0440**	**n_s = 1.158**	**0.9770**	**9.40**	**4.94**

3.7. Regeneration study

CS / SDOS adsorbed the most MBs and thus the most adsorption, so it was chosen to be evaluated using adsorption - desorption cycles five times in succession **Figure 9**. Each data point was collected three separate times and each set of results is expressed as means ± SD (n = 3) In the first adsorption/desorption cycle, there was about 95 % removal of MBs. This is represented as a dotted line at the bottom of the figure and represents the level of adsorption found in new CS/SDOS. After the first cycle of regeneration with 0.1M HCl, the percent MB removal dropped to 52.0 ± 1.06 %, then continued to drop until by the time of the fifth cycle the removal had dropped to 21.0 ± 0.56 %. Also, as can be seen in the graph, the amount of dye removed during desorption decreased from 60.0 ± 0.82 % to 40.0 ± 0.72 % by the time of the fifth cycle. Therefore, even though some measurable adsorption occurred after the five cycles, the fact that the removal efficiency dropped off so dramatically compared to the initial use of CS/SDOS indicates that the potential for practical reuse after multiple regeneration cycles with 0.1M HCl is limited. There are several factors that could have caused this reduction. First, there could have been some residual amounts of MB that were left on the surface of the adsorbent after acid-assisted desorption which could have reduced the availability of adsorption sites in future cycles. Second, the gradual reduction in desorption could suggest that more weakly bound dye was released into solution in previous cycles than strongly bound dye, resulting in smaller amounts being available for desorption later. Finally, the repeated exposure to HCl could potentially damage the chitosan matrix or reduce the noncovalent electrostatic and hydrophobic forces holding SDOS onto the surface of the chitosan and result in fewer anionic adsorption sites being available for future cycles. These reasons are speculative and cannot be proven since no characterization studies were done on the regenerated beads after they had been cycled through all five cycles. It would also be useful to measure any surfactants that might be released during those cycles. Therefore, further research would include looking at different regeneration agents or methods and characterizing the beads after cycling through many adsorption-desorption cycles (for instance by FTIR spectroscopy, morphologically, or by measuring surfactant release). Studies such as these will allow researchers to determine if a portion of MB is not desorbing due to structural changes in the chitosan matrix or if surfactant has leached out and whether either one of these is primarily responsible for the degradation of bead performance.

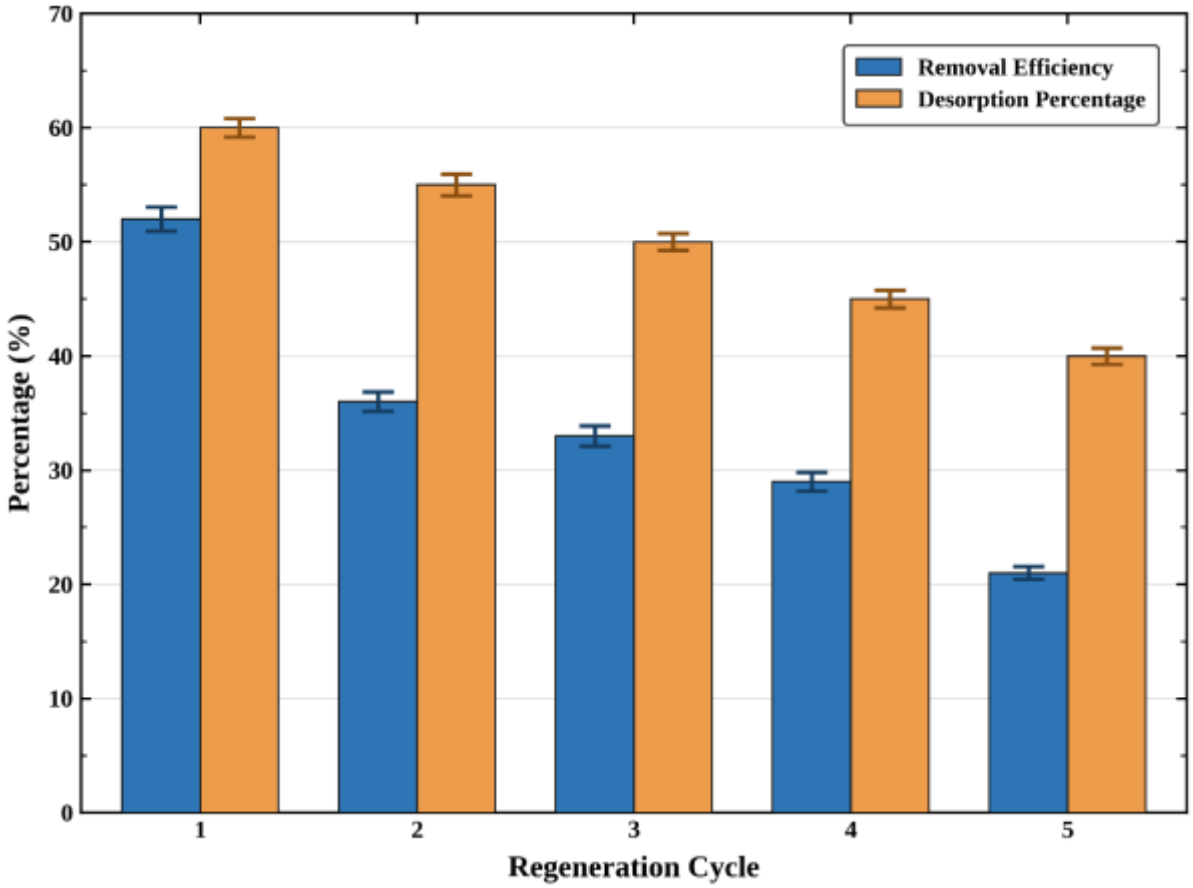


Figure 9. Removal efficiency and desorption percentage of MB for CS/SDOS after five regeneration cycles. Bars represent mean ± SD (n = 3). The dashed line denotes the fresh-adsorbent removal efficiency (95%) and is not a regenerated cycle. Adsorption conditions: C_0 = 100 mg L^{-1}, adsorbent dose = 0.02 g/40 mL, pH 6, 25 °C, 24 h, and no agitation. Regeneration conditions: 40 mL of 0.1 M HCl, 25 °C, and 60 min stirring.

4. Conclusion

This study compares chitosan hydrogel bead surfaces modified with three anionic surfactants [sodium dodecyl oleate sulfate (SDOS), sodium dodecyl sulfate (SDS), and sodium dodecyl benzene sulfonate (SDBS)] for removing methylene blue (MB) from aqueous solutions using the same experimental conditions. Qualitative evidence supporting the surface modifications was obtained by FTIR and FE-SEM; however, neither of these methods measured the amount of surfactant added per unit surface area nor the number of available adsorption sites. Since the BET surface area values were too small, and there was little correlation between the BET surface area and MB uptake, the physical adsorptive capacity alone cannot explain the observed adsorption. Surface modification at a surfactant concentration of 3.0 g/L resulted in significantly enhanced MB adsorption over unmodified chitosan. At pH = 6, each type of modified bead yielded higher MB uptakes. The pH dependency supports electrostatic interaction contributions to adsorption but establishes no additional information regarding the total adsorption mechanism. The MB adsorption performance on each bead followed the order CS/SDOS > CS/SDS > CS/SDBS, and the largest amounts of MB adsorbed on each bead were 418.60, 390.80, and 275.00 mg/g, respectively. The better-than-average performance of CS/SDOS might result from different organizations of surfactants on their respective surfaces and/or availability of anionic binding sites. Since neither measure has been taken directly to determine whether such mechanisms exist (i.e., whether the differences are due to variations in surface site density), they can be viewed as merely speculative explanations for these phenomena. A pseudo-second-order model provided the most accurate statistical descriptions of the kinetic data, where CS/SDOS demonstrated the greatest rapidity of initial MB uptake. However, the pseudo-second-order model does not demonstrate a chemisorption-based mechanism. A

Sips model provided the best overall fit to the equilibrium data. The Sips model's heterogeneity exponents demonstrated a higher degree of energy heterogeneity for both CS/SDOS and CS/SDS and Langmuir-type behavior for CS/SDBS. Model predictions for CS/SDOS (507.62 mg/g) and CS/SDS (445.03 mg/g) represent Sips capacities that exceed the maximum amount of MB adsorbed during experiments. Therefore, these values can be considered estimates based upon models. Furthermore, within the confines of its own model, CS/SDOS displayed the highest apparent affinity for MB. Affinity is not a measure of chemical bond strength. The comparative investigation of SDOS-, SDS-, and SDBS-modified chitosan beads prepared under the same conditions provides the primary contribution of this research and demonstrates that CS/SDOS is the most effective material examined in this research for MB adsorption. However, regeneration with 0.1 M HCl presented a practical problem since MB removal decreased from approximately 95% on freshly prepared materials to 52% after one cycle and 21% after five cycles. While measurable activity still existed after five cycles, the decrease limits reusability of CS/SDOS under current regeneration conditions. Possible reasons include incomplete dye desorption, changes in the chitosan matrix, and surfactant loss; however, none have been proven definitively. Quantification of surfactant loading and surface charge will provide further insight into the adsorption process, including by measuring sulfur content via elemental analysis, analyzing mass loss via thermogravimetry, determining mass balances for surfactant, obtaining zeta potentials, and determining the point of zero charge. Evaluation of milder or alternative regeneration media should also be performed along with post-cycling studies using FTIR spectroscopy, morphological examination, and measurements of surfactant release. These studies will allow clarification of the adsorption mechanism and facilitate development of a more stable and reusable form of CS/SDOS as an adsorbent.

Conflict of interest

The author declares no conflict of interest.

References

1. I. Anastopoulos, M. J. Ahmed, and E. H. Hummadi, “Eucalyptus-based materials as adsorbents for heavy metals and dyes removal from (waste)waters,” Jun. 15, 2022, *Elsevier B.V.* doi: 10.1016/j.molliq.2022.118864.
2. S. K. Ajjam, B. H. Hlih, and H. H. Alwan, “Enhancing lead ion removal from simulated wastewater through continuous electrocoagulation process: investigating operating parameters and adsorption behavior,” *Chemical Papers*, vol. 78, no. 18, pp. 9569–9579, 2024, doi: 10.1007/s11696-024-03771-1.
3. M. Vakili *et al.*, “Application of chitosan and its derivatives as adsorbents for dye removal from water and wastewater: A review,” Nov. 26, 2014, *Elsevier Ltd*. doi: 10.1016/j.carbpol.2014.07.007.
4. H. Kolya and C. W. Kang, “Toxicity of Metal Oxides, Dyes, and Dissolved Organic Matter in Water: Implications for the Environment and Human Health,” Feb. 01, 2024, *Multidisciplinary Digital Publishing Institute (MDPI)*. doi: 10.3390/toxics12020111.
5. B. A. Al-Mur and M. T. Jamal, “Eco-Friendly Dye Removal Using Chitosan: Characterization and Kinetic Modeling of Methylene Blue and Methyl Orange Adsorption,” *Polymers (Basel).*, vol. 18, no. 5, p. 546, Feb. 2026, doi: 10.3390/polym18050546.
6. I. Khan *et al.*, “Review on Methylene Blue: Its Properties, Uses, Toxicity and Photodegradation,” Jan. 01, 2022, *MDPI*. doi: 10.3390/w14020242.
7. N. M. Hosny, I. Gomaa, and M. G. Elmahgary, “Adsorption of polluted dyes from water by transition metal oxides: A review,” *Applied Surface Science Advances*, vol. 15, Jun. 2023, doi: 10.1016/j.apsadv.2023.100395.
8. M. J. Ahmed, “Preparation of activated carbons from date (Phoenix dactylifera L.) palm stones and application for wastewater treatments: Review,” Jul. 01, 2016, *Institution of Chemical Engineers*. doi: 10.1016/j.psep.2016.03.010.
9. M. J. Ahmed, B. H. Hameed, I. Anastopoulos, and W. A. Khanday, “Recent advances in surfactant-functionalized materials as adsorbents for enhanced remediation of synthetic dyes: A review,” Jan. 01, 2026, *Taiwan Institute of Chemical Engineers*. doi: 10.1016/j.jtice.2025.106398.
10. A. L. Cazetta *et al.*, “NaOH-activated carbon of high surface area produced from coconut shell: Kinetics and equilibrium studies from the methylene blue adsorption,” *Chemical Engineering Journal*, vol. 174, no. 1, pp. 117–125, Oct. 2011, doi: 10.1016/j.cej.2011.08.058.

11. M. J. Ahmed, “Application of agricultural based activated carbons by microwave and conventional activations for basic dye adsorption: Review,” Mar. 01, 2016, *Elsevier Ltd*. doi: 10.1016/j.jece.2015.10.027.
12. R. S. Dassanayake, S. Acharya, and N. Abidi, “Recent advances in biopolymer-based dye removal technologies,” Aug. 01, 2021, *MDPI AG*. doi: 10.3390/molecules26154697.
13. K. V. Harish Prashanth and R. N. Tharanathan, “Chitin/chitosan: modifications and their unlimited application potential-an overview,” Mar. 2007. doi: 10.1016/j.tifs.2006.10.022.
14. S. Chatterjee, D. S. Lee, M. W. Lee, and S. H. Woo, “Congo red adsorption from aqueous solutions by using chitosan hydrogel beads impregnated with nonionic or anionic surfactant,” *Bioresour. Technol.*, vol. 100, no. 17, pp. 3862–3868, Sep. 2009, doi: 10.1016/j.biortech.2009.03.023.
15. S. Chatterjee, T. Chatterjee, S. R. Lim, and S. H. Woo, “Adsorption of a cationic dye, methylene blue, on to chitosan hydrogel beads generated by anionic surfactant gelation,” *Environ. Technol.*, vol. 32, no. 13, pp. 1503–1514, 2011, doi: 10.1080/09593330.2010.543157.
16. M. Anbia, S. A. Hariri, and S. N. Ashrafizadeh, “Adsorptive removal of anionic dyes by modified nanoporous silica SBA-3,” *Appl. Surf. Sci.*, vol. 256, no. 10, pp. 3228–3233, Mar. 2010, doi: 10.1016/j.apsusc.2009.12.010.
17. M. Anbia, S. A. Hariri, and S. N. Ashrafizadeh, “Adsorptive removal of anionic dyes by modified nanoporous silica SBA-3,” *Appl. Surf. Sci.*, vol. 256, no. 10, pp. 3228–3233, Mar. 2010, doi: 10.1016/j.apsusc.2009.12.010.
18. F. Raji, M. Zafari, A. Rahbar-Kelishami, and S. N. Ashrafizadeh, “Enhanced removal of methyl orange using modified anion exchange membrane adsorbent,” *International Journal of Environmental Science and Technology*, vol. 20, no. 9, pp. 9823–9836, Sep. 2023, doi: 10.1007/s13762-023-05089-z.
19. S. Sorayyaei, F. Raji, A. Rahbar-Kelishami, and S. N. Ashrafizadeh, “Combination of electrocoagulation and adsorption processes to remove methyl orange from aqueous solution,” *Environ. Technol. Innov.*, vol. 24, Nov. 2021, doi: 10.1016/j.eti.2021.102018.
20. H. Farrokhzad *et al.*, “Novel composite cation exchange films based on sulfonated PVDF for electromembrane separations,” *J. Memb. Sci.*, vol. 474, pp. 167–174, Jan. 2015, doi: 10.1016/j.memsci.2014.10.002.
21. Z. Zhang *et al.*, “Efficient removal of anionic dyes by chitosan-based hydrogels modified with SDS and NaOH: Structural optimization, adsorption performance, and mechanistic insights,” *Int. J. Biol. Macromol.*, vol. 321, Sep. 2025, doi: 10.1016/j.ijbiomac.2025.146275.
22. G. Rando *et al.*, “Nanofiber PVA-Based Membranes Incorporating Functionalized Spanish Broom Derivatives for Sustainable Water Purification,” *Energy and Environmental Materials*, 2026, doi: 10.1002/eem2.70321.
23. L. Fu, J. He, B. Yang, Z. Zhang, and W. Gong, “Synthesis of chlorite-based magnetic composite for treatment of dodecylamine-containing beneficiation wastewater,” *Colloids Surf. A Physicochem. Eng. Asp.*, vol. 726, Dec. 2025, doi: 10.1016/j.colsurfa.2025.137796.
24. J. He, L. Zhu, S. Guo, and B. Yang, “An effective strategy for coal-series kaolin utilization: Preparation of magnetic adsorbent for Congo red adsorption,” *Chem. Eng. Sci.*, vol. 304, Feb. 2025, doi: 10.1016/j.ces.2024.120958.
25. R. Tayebee, E. Esmaeili, B. Maleki, A. Khoshniat, M. Chahkandi, and N. Mollania, “Photodegradation of methylene blue and some emerging pharmaceutical micropollutants with an aqueous suspension of WZnO-NH2@H3PW12O40 nanocomposite,” *J. Mol. Liq.*, vol. 317, Nov. 2020, doi: 10.1016/j.molliq.2020.113928.
26. A. Zamani, S. Asghari, and M. Tajbakhsh, “Synthesis of TiO2/CD and TiO2/Ag/CD Nanocomposites and Investigation of Their Visible Light Photocatalytic Activities in the Degradation of Methylene Blue,” *Chemical Methodologies*, vol. 8, no. 3, pp. 177–199, Mar. 2024, doi: 10.48309/chemm.2024.432168.1753.
27. M. R. Khanlary, E. Shaghagi Varzeghani, S. Rafiee, S. B. Chegini, and Z. Pasalari, “Chemical Methodologies Chemical Synthetization of MoS2 Nanofilm to Enhance Photocatalytic Degradation of Methylene Blue,” */ Chem. Methodol*, vol. 2026, no. 6, pp. 586–597, 2026, doi: 10.48309/chemm.2026.553496.2025.
28. S. Messa and S. Olfati, “Application of Manganese Oxide (MnO_2) Nanoparticles in Water Purification: Mechanisms of Chemical Pollutant Removal and Environmental Challenges,” vol. 3, pp. 62–76, 2025, doi: 10.22034/nc.2025.558983.1059.
29. S. Wang and H. Chen, “TiO_2/Graphene Nanocomposite Finishing for UV-Protective and Self-Cleaning Athletic Fabrics”, doi: 10.22034/nc.2026.584344.1090.
30. T. Sembiring *et al.*, “Synthesis and Characterization of Magnetic Fe3O4/TEOS/TiO2 Composites for Methylene Blue Photodegradation,” *Advanced Journal of Chemistry, Section A*, vol. 8, no. 5, pp. 930–947, May 2025, doi: 10.48309/ajca.2025.464679.1576.
31. D. Kurniawati, S. Kasuma Warda Ningsih, D. Beri, P. Ramadhani, L. Hevira, and M. Suciandica, “Advanced Journal of Chemistry, Section A Adsorption Performance of CTAB-Modified Longan Peel: A Sustainable Biosorbent for Rhodamine B and Methylene Blue Removal from Aqueous Systems,” *Advanced Journal of Chemistry, Section A*, vol. 2026, no. 11, pp. 2040–2052, 2026, doi: 10.48309/ajca.2026.579257.2097.

32. F. Firnanelty, A. Putri, K. R. Karim, S. Chadijah, and E. Jumrah, “Chemical Methodologies Green Synthesis of Bentonite-Hydroxyapatite from Eggshell Waste for Methylene Blue Dye Adsorption,” 2026, doi: 10.48309/chemm.2026.573179.2093.
33. D. Das and A. Pal, “Adsolubilization phenomenon perceived in chitosan beads leading to a fast and enhanced malachite green removal,” *Chemical Engineering Journal*, vol. 290, pp. 371–380, Apr. 2016, doi: 10.1016/j.cej.2016.01.062.
34. V. Herbert Freundlich, “Über die Adsorption in Lösungen 1).”
35. S. K. Ajjam, M. A. Aljaleel, B. H. Hlihl, and H. H. Alwan, “Nitrate removal from simulated wastewater by electrocoagulation: Impact of operating parameters on removal efficiency and energy consumption,” *S. Afr. J. Chem. Eng.*, vol. 55, pp. 1–10, 2026, doi: https://doi.org/10.1016/j.sajce.2025.10.002.
36. R. Sips, “On the structure of a catalyst surface,” *J. Chem. Phys.*, vol. 16, no. 5, pp. 490–495, 1948, doi: 10.1063/1.1746922.
37. N. Bagotia, “Regeneration strategies for exhausted adsorbents used in water treatment - A critical review,” Jan. 01, 2025, *Elsevier Ltd*. doi: 10.1016/j.jwpe.2024.106560.
38. A. El-Araby, W. Janati, R. Ullah, S. Ercisli, and F. Errachidi, “Chitosan, chitosan derivatives, and chitosan-based nanocomposites: eco-friendly materials for advanced applications (a review),” 2023, *Frontiers Media SA*. doi: 10.3389/fchem.2023.1327426.
39. X. Guo, Z. Zhao, X. Gao, Y. Dong, H. Fu, and X. Zhang, “Study on the adsorption performance of modified high silica fly ash for methylene blue,” *RSC Adv.*, vol. 14, no. 30, pp. 21342–21354, Jul. 2024, doi: 10.1039/d4ra04017a.
40. P. O. Oladoye, T. O. Ajiboye, E. O. Omotola, and O. J. Oyewola, “Methylene blue dye: Toxicity and potential elimination technology from wastewater,” Dec. 01, 2022, *Elsevier B.V.* doi: 10.1016/j.rineng.2022.100678.
41. M. Loutfi, R. Mariouch, I. Mariouch, M. Belfaquir, and M. S. ElYoubi, “Adsorption of methylene blue dye from aqueous solutions onto natural clay: Equilibrium and kinetic studies,” in Materials Today: Proceedings, Elsevier Ltd, Jan. 2023, pp. 3638–3643. doi: 10.1016/j.matpr.2022.08.412.